

Sustainable Generation of Ni(OH)₂ Nanoparticles for the Green Synthesis of 5-Substituted 1*H*-Tetrazoles: A Competent Turn on Fluorescence Sensing of H₂O₂

Mita Halder,[†] Md. Mominul Islam,[‡] Pritam Singh,[†] Anupam Singha Roy,^{*,§} Sk. Manirul Islam,^{*,‡} and Kamalika Sen^{*,†}

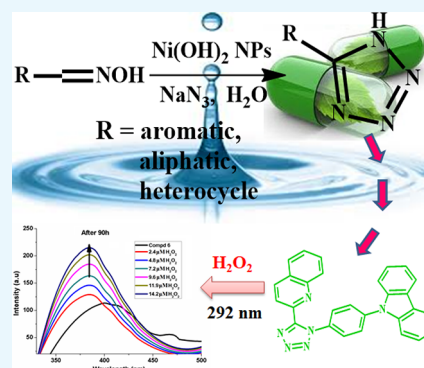
[†]Department of Chemistry, University of Calcutta, 92 APC Road, Kolkata 700 009, India

[‡]Department of Chemistry, University of Kalyani, Kalyani, Nadia 741235, West Bengal, India

[§]European Bioenergy Research Institute, Aston University, Birmingham B4 7ET, U.K.

S Supporting Information

ABSTRACT: A mutually correlated green protocol has been devised that originates from a sustainable production of β -Ni(OH)₂ nanoparticles which is used for an efficient catalytic synthesis of versatile substituted tetrazoles, under mild reaction conditions in water via a simple, one-pot, eco-friendly method. The synthesis is followed by derivatization into a highly fluorescence active compound 9-(4-(5-(quinolin-2-yl)-1*H*-tetrazol-1-yl)phenyl)-9*H*-carbazole that can be used at tracer concentrations (0.1 μ M) to detect as well as quantify hydrogen peroxide down to 2 μ M concentration. The nanocatalyst was synthesized by a simple, proficient, and cost-effective methodology and characterized thoroughly by UV–vis absorption and Fourier transform infrared spectra, N₂ adsorption/desorption, high resolution transmission electron microscopy, powder X-ray diffraction pattern, field emission scanning electron microscopy, and thermogravimetric analysis. Broad substrate scope, easy handling, higher efficiency, low cost, and reusability of the catalyst are some of the important features of this heterogeneous catalytic system. The strong analytical performance of the resultant derivative in low-level quantification of potentially hazardous hydrogen peroxide is the key success of the overall green synthesis procedure reported here.



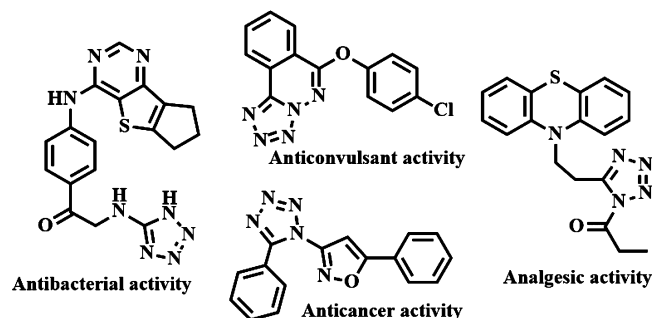
1. INTRODUCTION

Sustainable synthesis of nitrogen rich heterocycles has attracted growing interest over a decade. In this regard, tetrazoles, a group of five-membered ring compounds containing four nitrogen atoms, have received wide attention in recent years because of their vast and extraordinary activity in pharmaceutical and medicinal chemistry^{1–4} (Scheme 1). They also have a similar implementation in the field of industrial chemistry, chemistry of materials (including light sensitive agents, polymers, energy materials, various explosives,

etc.),^{5–9} and coordination chemistry.^{10,11} Furthermore, tetrazoles have a wide range of agricultural applications,^{12,13} for instance, they are used to control unwanted herbs and fungi and help to regulate the plant growth.

Because of these wide range of applications, development of an efficient synthetic route for tetrazole-based compounds is in vogue. In this context, numerous synthetic strategies are reported in the literature. After the pioneering work by Hantzsch and Vagt,¹⁴ a variety of modified procedures were developed, but majority of them were based on the addition of azides to the nitrile groups,^{15–20} while some groups have also used isocyanide,²¹ primary alcohols, aldehydes²² and so forth, in different toxic organic solvent media. All the reactions were carried out under homogeneous conditions using stoichiometric amount of metal catalysts,^{23,24} Lewis acids^{25–27} or ionic liquids.²⁸ Besides, there are a plethora of contributions related to diverse types of homogeneous catalytic systems reported in literature.^{29–33} However, use of expensive ligands and toxic organic solvents, probability of metal contamination in the products, application of additives, and finally lack of reusability

Scheme 1. Potent Molecules Bearing Tetrazole Skeleton



Received: May 22, 2018

Accepted: July 11, 2018

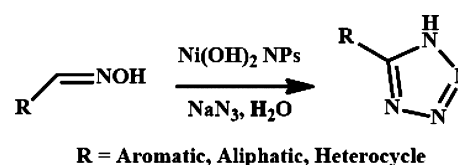
Published: July 23, 2018

of the catalyst demand serious attentions. An efficient greener alternative where the catalyst can be reused through an environment-friendly manner is therefore welcome. Very recently, some heterogeneous catalytic systems^{34–38} have also been developed to overcome these drawbacks. Till now, heterogeneous transition metal catalyzed synthetic pathways are one of the most interesting as well as challenging areas. In this context, nickel as a transition metal catalyst, creates a promising center of attraction toward the researchers. Nanoparticles (NPs), having unusually huge surface area and large number of active sites, can efficiently catalyze several organic reactions providing the advantages of high atom economy, mild reaction conditions, simplified isolation of product, easy recovery, and recyclability of the catalysts.^{39–41} Considering the ongoing attempts and increasing awareness to develop simple, environment-friendly, economic, and profitable synthetic methods, nickel-based NPs can serve as a powerful alternative.^{42,43} Incidentally, several reports are available in the literature regarding the synthesis of tetrazole compounds catalyzed by diverse type of nickel-based NPs.^{44–48} Moreover, aldoxime derivatives have captured the attention of synthetic organic chemists during the past few years^{49–51} because of their good reactivity and less toxic nature and the fact that they can be prepared very easily. Very recently, Patil,⁵² Babu,⁵³ and Matsugi⁵⁴ have reported, respectively, the homogeneous $\text{Cu}(\text{OAc})_2$, InCl_3 , and DPPA catalyzed synthesis of 5-substituted 1*H*-tetrazoles from aldoxime and sodium azide.

On the other hand, the past decade has witnessed a surge in the sensing application of several materials for ultratrace sensing of hydrogen peroxide because of multiple reasons.^{55–58} It is one of the most powerful oxidizing agents and is a proficient generator of reactive oxygen species.^{59,60} H_2O_2 has immense applications in the industrial and medicinal fields.^{61,62} Additionally, H_2O_2 is produced by all living cells upon reduction of O_2 by NADPH oxidase^{63,64} and by several other mechanisms also.^{65–68} Such production is believed to get enhanced with aging and other ailments.^{69–71} Moreover, it may enter the body system with certain beverages like instant coffee or sanitized water. Sensing of H_2O_2 in different samples of environmental, industrial, and biological importance at trace scale is therefore required together with suitable remediation methods. An extensive study of H_2O_2 sensing methods have been done by several researchers.^{72–76} The most popularly selected methods involve electrochemical techniques which entail special laboratory setup and requirements.^{77,78} Reports on spectral methods of H_2O_2 sensing are in severe dearth in recent days, despite their easy handling and measurement conditions.^{79,80}

In this context, we hope to introduce here a novel and efficient synthetic strategy of designing recyclable heterogeneous nickel hydroxide NPs to surmount several aforementioned obstructions in the synthesis of 5-substituted 1*H*-tetrazoles starting from aldoximes and sodium azide in water under mild reaction conditions (Scheme 2). Using our protocol, we finally end up in designing 9-(4-(5-(quinolin-2-yl)-1*H*-tetrazol-1-yl)phenyl)-9*H*-carbazole (compound 6) as a spin off. Only 0.1 μM concentration of this compound is potent enough for spectrofluorimetric sensing of trace concentrations of H_2O_2 . The overall synthesis methods and the sensing experiments have been performed in green solvent media utilizing hassle free techniques and hazard free reagents. A comparison of the present sensing method as well as the

Scheme 2. Synthetic Scheme of 5-Substituted 1*H*-Tetrazoles from Aldoxime



efficacy of the catalytic activity of the $\text{Ni}(\text{OH})_2$ NPs with the literature is presented in Tables S1 and S2 respectively in the Supporting Information.

2. RESULTS AND DISCUSSION

2.1. Characterization of the $\text{Ni}(\text{OH})_2$ NPs. Nickel hydroxide NPs were prepared by refluxing nickel acetate and sodium hydroxide in ethanol in the presence of catalytic amount of acetic acid for 1.5 h (Scheme 3). The hydroxide NP formation in this case is assisted by acetic acid, which helps to generate nanodimensional mesoporous $\text{Ni}(\text{OH})_2$ NPs.^{81,82} The instantaneous hydroxide precipitation due to the addition of NaOH in the medium is hindered by the presence of acetic acid; hence, a slow rate of hydroxide formation results in the generation of multiple nucleation sites with small particles in the nanostate. A molar ratio of 2.5:1 of alkali to acid in the medium was found to be most suitable for the generation of nanodimensional particles in the solution.⁸² For characterization, the as-synthesized NPs were analyzed by powder X-ray diffraction (PXRD), diffuse reflectance spectroscopy (DRS)-UV and Fourier transform infrared (FTIR) spectroscopy, scanning electron microscopy (SEM), transmission electron microscopy (TEM), N_2 adsorption/desorption, and thermogravimetric analysis (TGA).

2.1.1. PXRD and N_2 Adsorption/Desorption Isotherm. The phase composition and form of the newly synthesized nickel hydroxide were examined by PXRD analysis (Figure 1a). All the diffraction peaks are in good agreement with the hexagonal $\beta\text{-Ni}(\text{OH})_2$ with lattice constants $a = 3.12$ and $c = 4.6$ Å (JCPDS no. 14-0117). Figure 1b represents the PXRD pattern of the reused $\beta\text{-Ni}(\text{OH})_2$ NPs (after fifth cycle). The specific surface area and porous nature of $\text{Ni}(\text{OH})_2$ NPs were measured from Brunauer–Emmett–Teller (BET) gas-adsorption measurements. N_2 adsorption/desorption isotherm of the porous nickel hydroxide NPs is shown in Figure 2a, and the corresponding Barrett–Joyner–Halenda (BJH) pore size distribution plot is given in Figure 2b. The catalyst shows an isotherm similar to type IV, characteristic of mesoporous materials, and the hysteresis loop is of type H1. The BET specific surface area of the material was found to be $160.5 \text{ m}^2 \text{ g}^{-1}$. The average pore diameter according to the BJH plot calculated from the N_2 desorption isotherm was 3.87 nm, indicating that the sample has mesoscale pores.

2.1.2. DRS-UV and FTIR Spectral Analysis. Figure 3a shows absorption spectrum of the $\beta\text{-Ni}(\text{OH})_2$ in the UV and visible region. $\beta\text{-Ni}(\text{OH})_2$ showed an absorption maximum at 245 nm which is attributed to band gap absorptions in $\beta\text{-Ni}(\text{OH})_2$.⁸³ The absorption spectra exhibit three bands at 312, 386 nm, and a broad band centered at 670 nm for $\beta\text{-Ni}(\text{OH})_2$, which are governed by the d–d transitions. The FTIR spectra of the synthesized $\beta\text{-Ni}(\text{OH})_2$ NPs are shown in Figure 3b. The strong absorption at 521 cm^{-1} is due to Ni–O–H bending and Ni–O stretching vibrations. The band at 1632 cm^{-1} is assigned to the bending vibration for absorbed water molecule. The

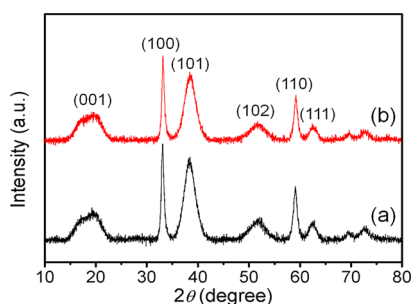
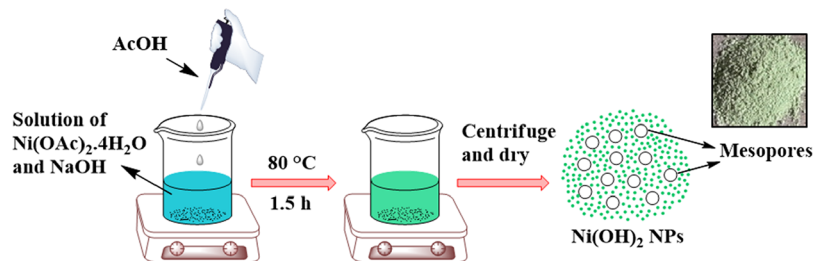
Scheme 3. Schematic Diagram for the Synthesis of Ni(OH)₂ NPs

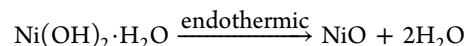
Figure 1. PXRD patterns of (a) fresh β -Ni(OH)₂ NPs and (b) reused β -Ni(OH)₂ NPs.

sharp peak at 3645 cm^{-1} corresponds to the stretching vibration mode of nonhydrogen-bonded hydroxyl groups. The broad band centered at 3429 cm^{-1} can be attributed to the stretching vibration of water molecules in the nickel hydroxide material.

2.1.3. Field-Emission SEM (FESEM) and High Resolution TEM (HRTEM) Analysis. Figure 4 shows the SEM images of Ni(OH)₂ NPs. The images indicate good uniformity of the Ni(OH)₂ material, and these NPs have a uniform average size below 10 nm. Figure 5a represents the HRTEM images of β -Ni(OH)₂. Here, the NPs are in 5–10 nm range in diameter (Figure 5b) while the pore diameter is in 3–4 nm range. The average particle size was estimated from the PSD plot (Figure 5b) and was found to be 7.6 nm. Mesopores are created during nucleation and agglomeration of the NPs and are generated out of the interconnected NPs forming interparticle spaces. TEM image of recycled β -Ni(OH)₂ (after third run) is given in Figure 5c.

2.1.4. Thermogravimetry (TG)–Differential Thermal (DTA) Analyses. The thermal behavior of β -Ni(OH)₂ NPs was investigated using TG and DT measurement (Figure 6). The TG curve showed that β -Ni(OH)₂ started to decompose slowly after 100 °C. The major weight loss happened between 220 and 450 °C. The total weight loss was measured to be

32.44% (calculated value 32.51%). The DT curve showed an endothermic peak with a maximum located at 296 °C, corresponds to endothermic behavior during the decomposition of β -Ni(OH)₂ to NiO. The thermal decomposition process can be represented as



2.2. Synthesis of Tetrazoles from Aldoximes and Sodium Azide Using Ni(OH)₂ NPs.

A number of reactions were performed to optimize the reaction conditions with variation of diverse factors, viz., amount of catalyst, solvent, base, and temperature for the representative reaction of benzaldehyde oxime (1a) and sodium azide. The whole scenario is presented in Table 1. The reaction cannot be performed without any catalyst (Table 1, entry 1), which clearly indicates its synthetic importance. Then, the reaction was performed with the variation of solvents, bases, and temperature. The reaction gave poor-to-moderately good yields in DMF, toluene, *p*-xylene, and dioxane and in neat condition (Table 1, entry 2–6). However, among all the solvents, best yield was obtained from the water medium. It was also found that K₂CO₃ produced the best result amongst Cs₂CO₃, NaHCO₃, Na₂CO₃, and K₃PO₄ (Table 1, entry 10–13). Because the reaction was not proceeding at room temperature, all the reactions were carried out under refluxing conditions (Table 1, entry 8–9). Overall, the best yield resulted with 4.32 mol % of Ni(OH)₂ NPs in water after refluxing at 100 °C for 10 h under air (Table 1, entry 7).

After the attainment of the optimum conditions, we tried to explore the scope and efficacy of the newly generated catalyst and methodology to furnish the diversely substituted tetrazoles. It is found that aromatic aldoximes efficiently underwent this reaction to produce excellent product yields. The concise results are clearly represented in Table 2. This protocol is equally compatible with the substrates having both electron donating (–Me, –OH, –OMe) as well as electron withdrawing (–Cl, –Br, and –NO₂) groups, giving well-to-

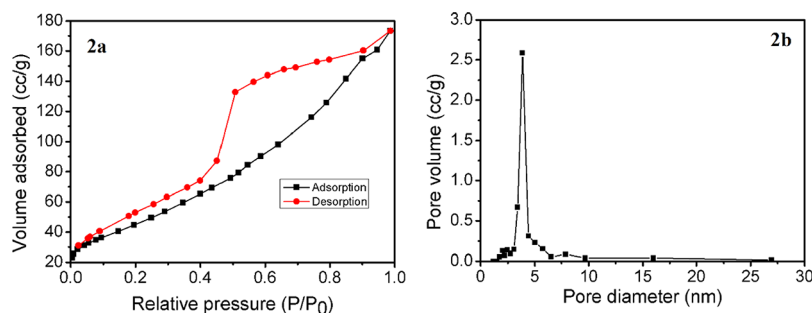


Figure 2. (a) N₂ adsorption/desorption isotherm and (b) power spectral density (PSD) curve of β -Ni(OH)₂.

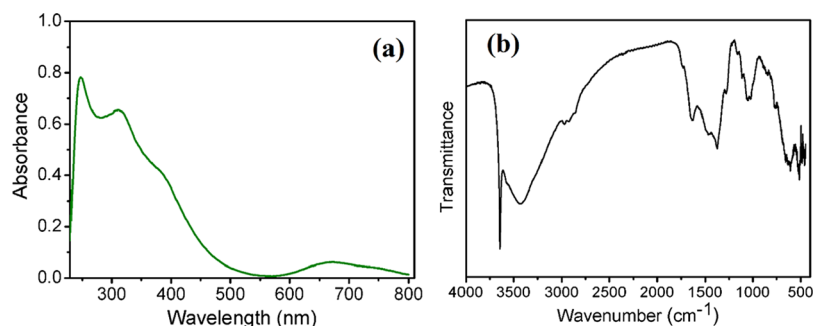


Figure 3. (a) Solid state UV-vis spectra and (b) FTIR spectra of β -Ni(OH)₂ NPs.

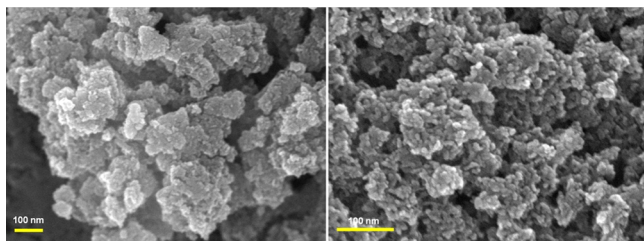


Figure 4. SEM images of β -Ni(OH)₂ NPs.

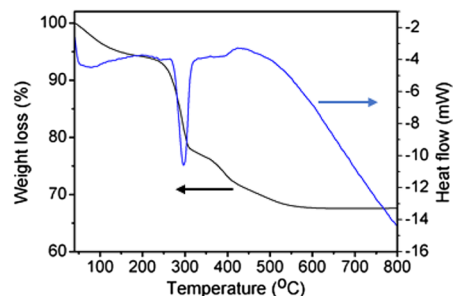


Figure 6. TG-DTA of the β -Ni(OH)₂.

excellent product yields. All the *o*-, *m*-, and *p*-nitro benzaldehyde oximes underwent this reaction efficiently giving the corresponding 5-substituted tetrazoles (Table 2, 2c, 2d, 2e) in good-to-excellent yields. Next, chloro- and bromo-substituted benzaldehyde oxime smoothly reacted with the azide to furnish the corresponding tetrazoles (Table 2, 2f, 2g, 2h) with very good yields. These observations undoubtedly signify the sensitivity and compatibility of this protocol. Next, 3,4-dimethoxy benzaldehyde oxime provided 5-(3,4-dimethoxyphenyl)-1*H*-tetrazole (Table 2, 2i) in 91% yield. Furthermore, a variety of hydroxyl-substituted benzaloximes also went through these reaction conditions providing the respective products (Table 2, 2k, 2l, 2m) with very good yields.

Next, the applicability of this technique was extended for the reaction between heterocyclic aldoximes and azide. Table 3 clearly represented the results. Furan-2-carbaldehyde oxime, thiophene-2-carbaldehyde oxime, and pyridine-2-carbaldehyde oxime effortlessly underwent this reaction to produce 3a, 3b, and 3c with 89, 91, and 93% yields. Likewise, quinoline-2-carboxaldehyde oxime and indole-3-carbaldehyde oxime gave the products (Table 3, 3d, 3e) with very good yields.

After achieving the remarkable success in application of our methodology in case of aromatic as well as heterocyclic

aldoximes, we tried to extend the scope in case of aliphatic aldoximes also. The results are summarized in Table 4. Formaldehyde oxime and heptanal oxime efficiently reacted with sodium azide to give the respective tetrazoles (Table 4, 4a, 4b) with moderate-to-good yields (75 and 72% yields). (2*E*)-Cinnamaldehyde oxime underwent this reaction with complete retention of configuration giving the corresponding (*E*)-5-styryl-1*H*-tetrazole (Table 4, 4c) as a sole product (selectivity ratio of *E/Z* is equal to 100:0). Once more, this observation evidently highlights the specificity of our methodology.

The synthetic importance of our current catalytic protocol was further examined through the synthesis of 9-(4-(5-(quinolin-2-yl)-1*H*-tetrazol-1-yl)-phenyl)-9*H*-carbazole (compound 6). The synthetic pathway is represented in Scheme 4. Herein, 9-(4-iodophenyl)-9*H*-carbazole (compound 5) was prepared from carbazole and 1,4-diiodo benzene with 85% yield. Thereafter, an efficient C–N cross-coupling reaction between 2-(1*H*-tetrazol-5-yl)-quinoline (Table 3, 3d) and compound 5 produced compound 6 with 89% of yield.

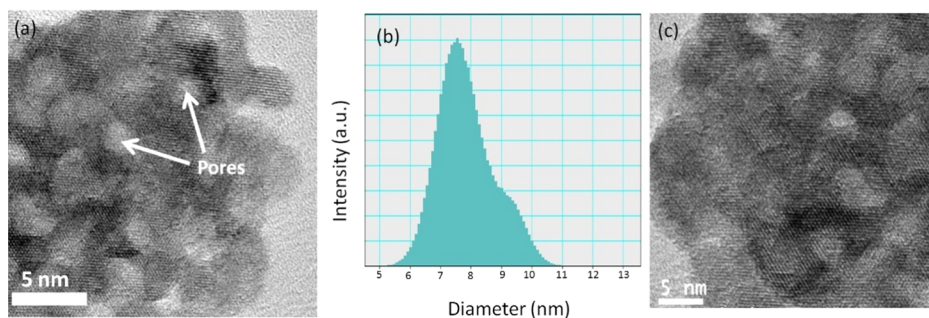
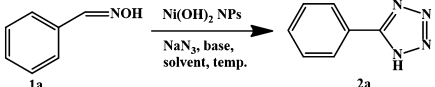
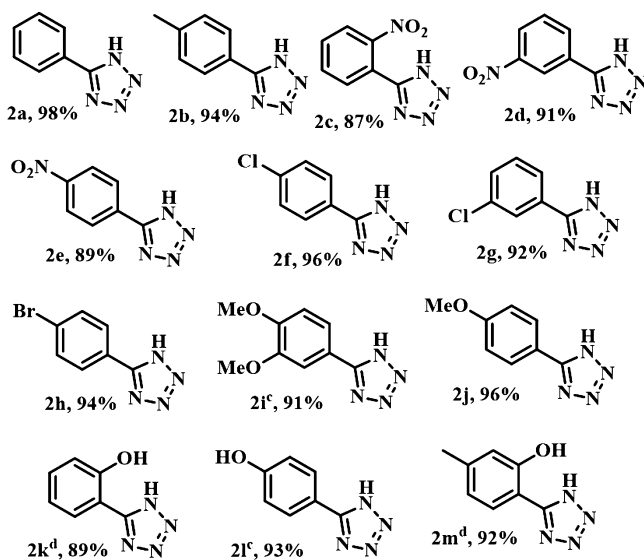


Figure 5. (a) HRTEM micrograph of fresh β -Ni(OH)₂ NPs, (b) particle size distribution of β -Ni(OH)₂, and (c) HRTEM micrograph of reused β -Ni(OH)₂ NPs.

Table 1. Optimization of Reaction Conditions^a


| entry | Cat. (mol %) | solvent | base | temp (°C) | yield (%) ^b |
|-------|--------------|------------------|---------------------------------|-----------|------------------------|
| 1 | | | K ₂ CO ₃ | 120 | |
| 2 | 4.32 | DMF | K ₂ CO ₃ | 120 | 30 |
| 3 | 4.32 | <i>p</i> -xylene | K ₂ CO ₃ | 120 | 83 |
| 4 | 4.32 | toluene | K ₂ CO ₃ | 110 | 56 |
| 5 | 4.32 | dioxane | K ₂ CO ₃ | 105 | 22 |
| 6 | 4.32 | | K ₂ CO ₃ | 120 | 52 |
| 7 | 4.32 | water | K ₂ CO ₃ | 100 | 98 |
| 8 | 4.32 | water | K ₂ CO ₃ | 65 | 38 |
| 9 | 4.32 | water | K ₂ CO ₃ | rt | |
| 10 | 4.32 | water | NaHCO ₃ | 100 | 68 |
| 11 | 4.32 | water | Cs ₂ CO ₃ | 100 | 32 |
| 12 | 4.32 | water | K ₃ PO ₄ | 100 | 23 |
| 13 | 4.32 | water | Na ₂ CO ₃ | 100 | 72 |
| 14 | 8.6 | water | K ₂ CO ₃ | 100 | 93 |

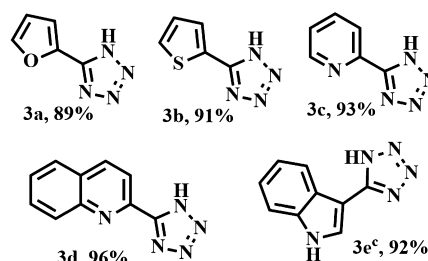
^a1a (1.0 mmol), NaN₃ (1.5 mmol), base (3.0 mmol), solvent (3.0 mL), Ni(OH)₂ NPs, 10 h. ^bYields are obtained by gas chromatography.

Table 2. Substrate Scope for Aromatic Aldoximes^{a,b}

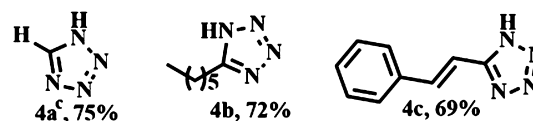
^aAromatic aldoximes (1.0 mmol), NaN₃ (1.5 mmol), K₂CO₃ (3.0 mmol), catalyst (4 mg, 4.32 mol %), water (3.0 mL), 10 h, reflux. ^bNMR spectra are given in the Supporting Information (Figures S1–S12). ^c12 h was required. ^d15 h time was required.

The compound **6** was found to have potential spectral features for sensing applications. The UV–vis absorption spectrum showed a prominent λ_{\max} at a wavelength of 292 nm with a considerable absorption intensity of a 0.057 μM solution (solution B) (Figure 7). The same solution upon excitation at this wavelength shows an emission maximum at $\lambda_{\text{em}} = 384$ nm. The fluorescence yield (ϕ_f) of the compound was calculated using a standard comparative method and was found to be 0.09% against a standard tryptophan solution.

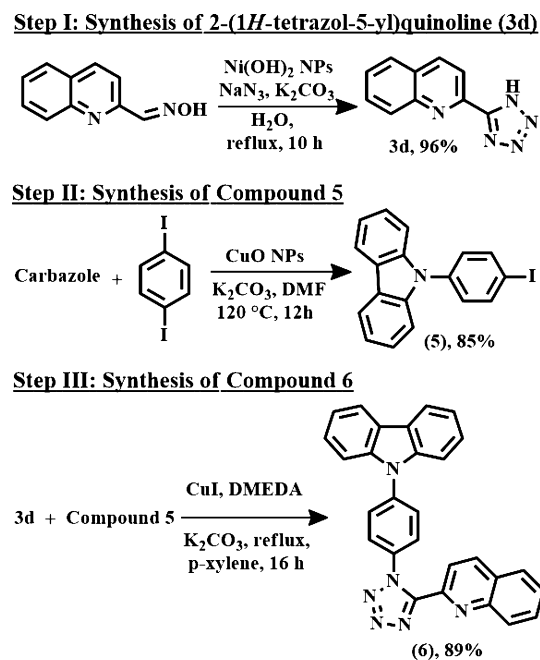
2.3. Spectral Sensing of Hydrogen Peroxide. The absorption intensity at the λ_{\max} position of 292 nm of the aforesaid solution of compound **6** (solution B) shows a gradual increase with increasing concentration of H₂O₂ solution (2–19

Table 3. Substrates for Heteroaromatic Aldoximes^{a,b}

^aHeteroaromatic aldoximes (1.0 mmol), NaN₃ (1.5 mmol), K₂CO₃ (3.0 mmol), catalyst (4 mg, 4.32 mol %), water (3.0 mL), 10 h, reflux. ^bNMR spectra are given in the Supporting Information (Figures S13–S16). ^c12 h was required.

Table 4. Substrate Scope for Aliphatic Aldoximes^{a,b}

^aAliphatic aldoximes (1.0 mmol), NaN₃ (1.5 mmol), K₂CO₃ (3.0 mmol), catalyst (4 mg, 4.32 mol %), water (3.0 mL), 18 h, reflux. ^bNMR spectra are given in the Supporting Information (Figures S17–S19). ^cWater: 1.5 mL.

Scheme 4. Schematic Route of Compound **6**

mM) (Figure 7). This UV–vis absorption of the compound at this wavelength corresponds to $n \rightarrow \pi^*$ transitions, which originate from the nonbonded electron pairs of nitrogen to the antibonding π orbitals of the aromatic moiety. On treatment with H₂O₂, some oxidative reactions generate bond cleavage,^{84,85} resulting in higher concentration of nonbonded electron density, and hence, a gradual increase in the absorbance value is observed (Figure 7). The fluorescence emission of solution A (higher concentration of compound **6** was required for emission quenching studies as compared to UV–vis absorption spectral studies) was measured upon instantaneous addition of H₂O₂, which shows a reverse trend

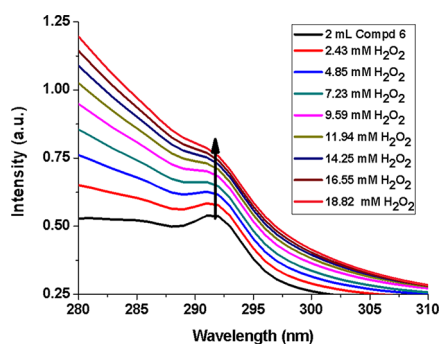


Figure 7. UV-vis absorption spectra of compound 6 in the presence of hydrogen peroxide.

with increasing H_2O_2 concentration in the range 2–16 mM. This is an obvious observation as the π conjugation decreases due to bond disruptions with increasing oxidation by H_2O_2 (Figure 8). The resulting Stern–Volmer plot (inset of Figure 8) shows a steady increase in the F_0/F value with increasing H_2O_2 concentration with a slope of $39 \text{ M}^{-1} \text{ L}$ (K_{SV}), indicating steady state interactions of the species with the fluorophore. The effect is also observed in the fluorescence lifetime of the compound, which suffers slight decrease (from 3.42 to 2.96 ns) upon oxidation with H_2O_2 (Figure 9).

The most interesting part of the emission-based experiments was observed when a much lower concentration of H_2O_2 was used to treat the solution of compound 6 (solution A). Instant addition of H_2O_2 solutions at lower concentrations (2.4–14.2 μM) could not create observable changes in the emission spectrum of solution A. However, a remarkable hike in the emission intensity of solution A treated with H_2O_2 of such low concentration was observed, if the solutions were allowed to rest for some time in the dark. Figure 10 shows a spectacular increase in the emission intensity of solution A treated with 4.8 μM H_2O_2 with increasing time interval. This observation is particularly important as the lower limit of detection of H_2O_2 becomes even lower, and enhanced emission intensities are observed instead of quenching which has much less specificity for analytes. The reason behind such observations depends on the fact that H_2O_2 initiates free radical reactions which involve many rearrangement steps, thereby reassembling the fragments of oxidation in a way that creates larger population of

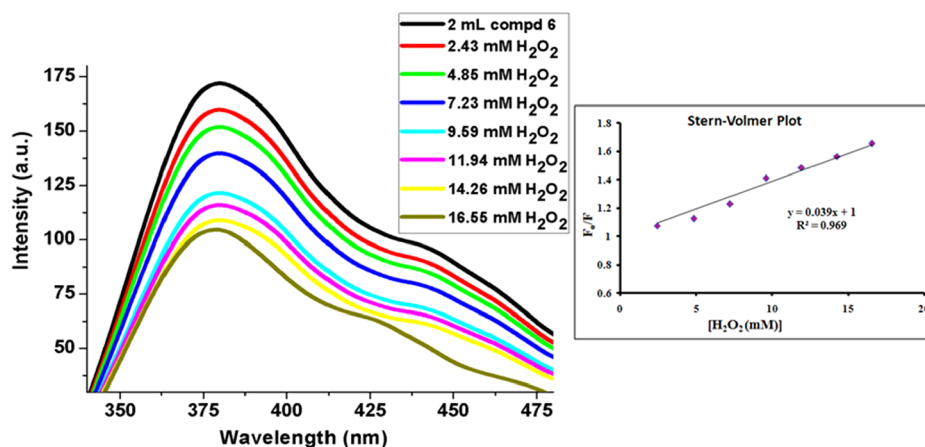


Figure 8. Fluorescence spectra and S–V plot of compound 6 in the presence of H_2O_2 .

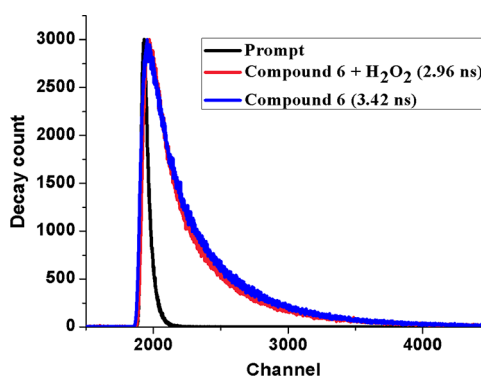


Figure 9. Fluorescence decay of compound 6 and H_2O_2 -treated compound 6 with time.

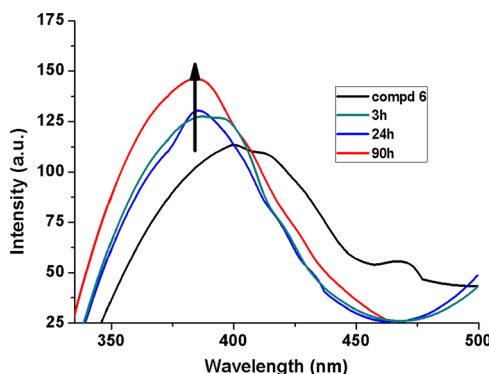


Figure 10. Fluorescence spectra of compound 6 and H_2O_2 -treated compound 6 with increasing intervals of time.

fluorophores and hence enhanced emission intensity with increasing time.

We have measured the emissions of solution A containing 2.4–14.2 μM H_2O_2 after keeping the systems in the dark for 3, 24, and 90 h (Figure 11) and plotted their respective F_0/F versus concentrations (inset of Figure 11) to obtain the slopes which showed an increasing trend in magnitude (−0.021, −0.022, and −0.037) with time. This reveals that higher sensitivity of the method is expected with longer duration of rest. The limit of detection for H_2O_2 observed here is compared with some literature reports in Table S1.

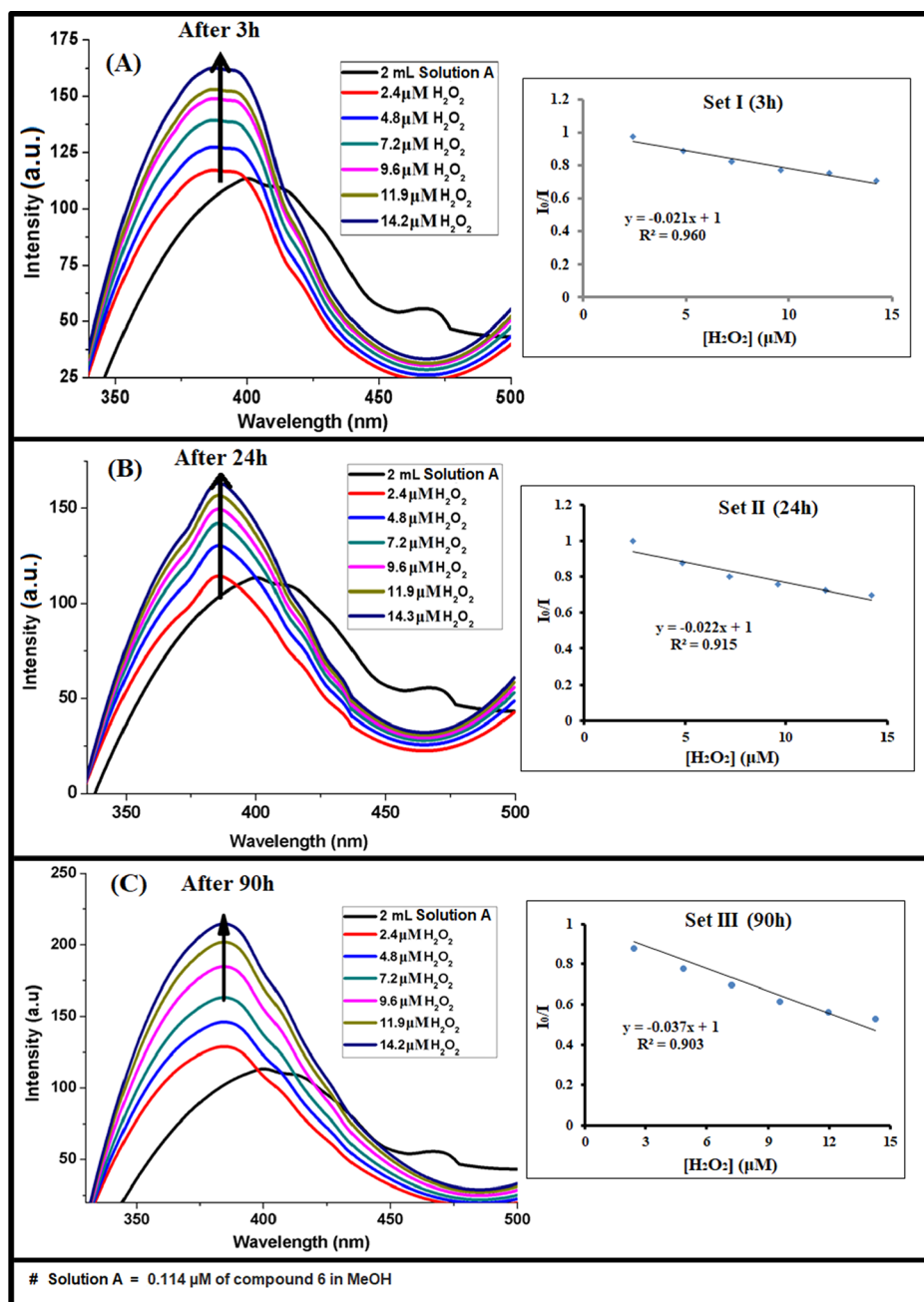


Figure 11. Fluorescence spectra of compound 6 and H_2O_2 -treated compound 6 after 3 h (A), 24 h (B), and 90 h (C). I_0/I vs $[H_2O_2]$ plots are the given inset.

The cyclic voltammogram (Figure 12) clearly indicates the redox activity of compound 6. It is notable that the reduction peaks (-1.66 and -1.007 V) appear along with oxidation peaks (1.468 and 1.664 V), which supports that the compound is easily oxidizable by hydrogen peroxide with reduction potential (1.776 V). Therefore, it can also be deduced that H_2O_2 undergoes easy reduction to H_2O during this redox process.

The viability of the results is further strengthened by performing the mass analysis using electrospray ionization (ESI-MS) technique. Figures S22 and S23 represent the ESI-MS spectra of the compound 6 and H_2O_2 -treated compound 6, respectively. The results are summarized in Table 5. The results clearly indicate that compound 6 undergoes different types of oxidative bond cleavage upon treatment with

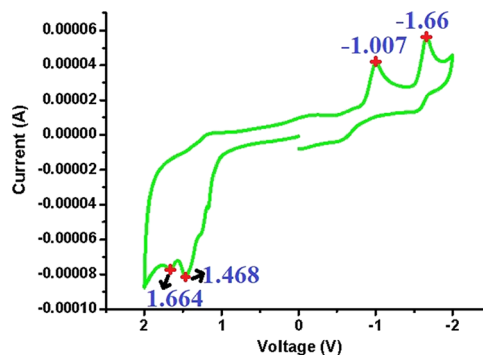


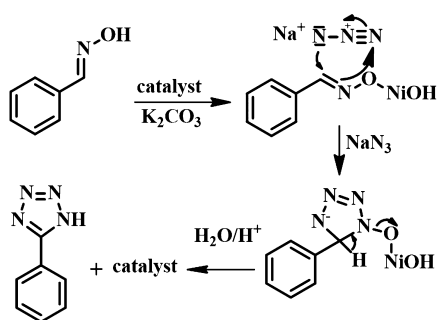
Figure 12. Cyclic voltammogram of compound 6.

Table 5. HRMS Data of Compound 6 and H₂O₂-Treated Compound 6

| compound | probable fragment | <i>m/z</i> |
|---|---|-----------------------------|
| compound 6 | [C ₂₈ H ₁₉ N ₆] ⁺ | 439 ([M + H] ⁺) |
| | [C ₂₈ H ₁₈ N ₄] ^{+•} | 410 |
| H ₂ O ₂ -treated compound 6 | [C ₂₈ H ₁₈ N ₄] ^{+•} | 410 |
| | [C ₁₈ H ₁₂ N ₄] ^{••} | 284 |
| | [C ₁₈ H ₁₂ N] ⁺ | 242 |
| | [C ₁₀ H ₆ N ₂] ^{••} | 154 |
| | [C ₉ H ₆ N] ⁺ | 128 |
| | [C ₂₈ H ₁₈ N ₃] ⁺ | 396 |

H₂O₂.^{84,85} The compound 6 (C₂₈H₁₈N₆), initially having a base peak at *m/z* 439 for the [M + H]⁺ species undergoes elimination of N₂ ("A" in Figure S22) to generate a peak at *m/z* 410. With H₂O₂-treated compound, the base peak now comes at *m/z* 410. The most plausible products of oxidative bond cleavage result in elimination of mass fragments with *m/z* 284 (for [C₁₈H₁₂N₄]^{••}), 242 (for [C₁₈H₁₂N]⁺), 154 (for [C₁₀H₆N₂]^{••}), and 128 (for [C₉H₆N]⁺) from compound 6 which can be clearly observed in the ESI-MS spectrum (in Figure S23).

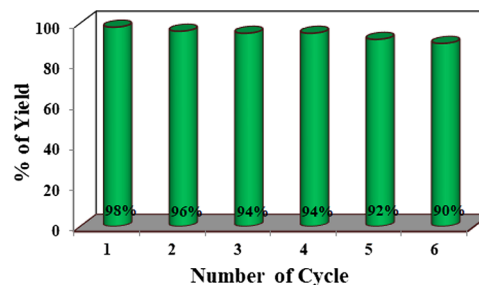
After getting excellent results upon application of our newly synthesized nanocatalyst, a preliminary investigation was undertaken to realize the mechanism. The conversion of benzaldoxime to benzonitrile in the absence of sodium azide was checked in the presence of the nickel hydroxide nanocatalyst, which did not take place under refluxing conditions in water. After 24 h, we get back the corresponding aldoxime without formation of benzonitrile. This observation clearly indicates that nitrile formation is not necessary in our methodology. The most probable reaction pathway is represented in Scheme 5.^{52–54} Initially, the Ni(OH)₂ NPs

Scheme 5. Possible Reaction Mechanism

bind with the oxygen atom of the aldoxime to activate the C=N bond. Then, azide ion undergoes cycloaddition with the activated imine bond. The cycloaddition between the C=N bond of aldoxime and azide takes place readily and form an intermediate. After removing the catalyst followed by acidic work-up, the desired product 5-substituted-1H-tetrazole was obtained.

2.4. Recyclability and Reusability of the Ni(OH)₂ Nanocatalyst. Recyclability, commencement, and thermal strength are the most important traits of a heterogeneous catalyst. Hence, to estimate the possibility to recover and reuse the nanocatalyst a model reaction between benzaldoxime and sodium azide was performed under optimal reaction conditions. At the end of the reaction, the catalyst was recovered through centrifugation, followed by washing with

water, ethyl acetate, and finally ethanol. Then, the catalyst was dried at 80 °C for activation. Figure 13 represents that the

**Figure 13.** Recyclability chart of the β -Ni(OH)₂ NPs.

catalyst can be reused successfully for six times without noticeable loss in the product yields. This fact is established by PXRD pattern (Figure 1b, after the fifth cycle), HRTEM (Figure 5c, after the third run) and FTIR (Figure S24, after the sixth cycle) study of the reused catalyst.

In a wider perspective, our newly generated methodology will make available a podium for the design of a sustainable and efficient synthetic route for 5-substituted 1H-tetrazoles. In nutshell, our catalytic system offers far better results as compared to other literature reports. This fact is clearly supported by the comparative study with the literature reports (Table S2, Supporting Information).

3. CONCLUSIONS

In conclusion, we have developed an efficient green and atom-economic novel synthetic route for the synthesis of 5-substituted 1H-tetrazoles starting from various aromatic, heterocyclic, as well as aliphatic aldoximes under mild reaction conditions in the presence of highly active and thermally stable, considerably recyclable Ni(OH)₂ NPs in water as a green solvent. The catalyst showed excellent catalytic activity because of its nanocrystalline nature, small particle size, large surface area, and good thermal stability. The synthetic protocol proffers various advantages, viz. good-to-excellent product yields, easy separation of catalyst, simple work-up, and eco-friendly methodology. Besides, using this protocol as one of the key steps, a fluorescent probe 9-(4-(5-(quinolin-2-yl)-1H-tetrazol-1-yl)-phenyl)-9H-carbazole was synthesized which is used at trace concentrations for the "turn on" spectral sensing of hydrogen peroxide at low concentrations. To the best of our familiarity, reports regarding the heterogeneous Ni(OH)₂ NPs catalyzed synthesis of 5-substituted 1H-tetrazoles from aldoximes are in severe dearth.

4. EXPERIMENTAL SECTION

4.1. Materials. Ni(OAc)₂·4H₂O (Sigma-Aldrich), H₂O₂ (Merck), and all other chemicals required for this study were used as received. All solvents were used after distillation and drying, following the standard procedure.

4.2. Instruments and Apparatus. Hermle microprocessor-controlled high-speed table-top centrifuge (model Z 36 K) was used for centrifugation. The FTIR spectra of the samples were recorded in the range 400–4000 cm⁻¹ on a PerkinElmer FTIR 783 spectrophotometer after pelletization using KBr. TEM images were obtained using a JEM 2100 transmission electron microscope. The surface morphology of the nanocatalyst was analyzed using a scanning electron

microscope (Zeiss EVO40, UK) equipped with an energy dispersive X-ray spectrometry facility. Surface area, pore size distribution, and mesopore volume were determined by N_2 porosimetry using Quantasorb Nova 4000e and 4200e porosimeters and Quanta chrome Novawin1.0 software upon sample outgassing in vacuo at 120 °C for 2 h. Specific surface area was calculated by applying the BET model. Pore size distributions and mesopore volumes were calculated by applying the BJH model to the desorption branch of the isotherm. PXRD patterns were recorded on a Bruker D8 ADVANCE diffractometer fitted with a Lynx Eye high-speed strip detector and a Cu $K\alpha$ source (1.54 Å, 8.04 keV). TGA was done using a Mettler Toledo TGA/DSC1 Star System under a N_2 purge gas (60 cm³ min⁻¹). The fluorescence study was done using a PerkinElmer LS-55 spectrofluorimeter equipped with a quartz cell with a 1.0 cm optical path length. The UV–vis absorption spectral study was performed using an Agilent 8453 diode array spectrophotometer. HORIBA Jobin Yvon Fluorocube 01-NL and 291 nm HORIBA nano-LED, IBH DAS-6 decay analysis software was used for time correlated single photon counting (TCSPC) lifetime spectroscopy. A Bioanalytical System EPSILON electrochemical analyzer was used for the cyclic voltammetric (CV) measurements. The measurements were carried out in the methanol medium, with a three-electrode assembly consisting of a glassy carbon disk working electrode, a platinum auxiliary electrode, and an aqueous Ag/AgCl reference electrode. All the ESI–MS spectra were recorded in a WATERS Xevo G2-SQToF instrument. The reactions were performed in a 10 mL round-bottomed flask fitted with a condenser under air. Thin-layer chromatography (TLC)-analysis was performed on TLC silica gel 60 F₂₅₄. The products were purified using silica gel (60–120 mesh) column chromatography. NMR spectra were recorded on a 400 MHz NMR instrument using CDCl₃ and DMSO-*d*₆ as solvents. The ¹H chemical shifts are reported in ppm relative to TMS. Carbon, hydrogen, and nitrogen contents of all products were examined utilizing a PerkinElmer 2400 Series II CHN analyzer.

4.3. Synthesis of Nickel Hydroxide NPs. To an ethanolic solution of Ni(OAc)₂·4H₂O (1.2 mmol, 40 mL), ethanolic solution of NaOH (2.5 mmol, 20 mL) was added. Then, after addition of 0.15 mL glacial acetic acid to it, the resulting mixture was refluxed for 1.5 h. After cooling, the as-synthesized NPs were separated from the solution through centrifugation at 6000 rpm for 8 min followed by redispersion in ethanol till the pH becomes neutral. Finally, the catalyst was dried in an oven at 60 °C for 3 h. Scheme 3 represents the schematic diagram for the synthesis of Ni(OH)₂ NPs.

4.4. General Procedure for the Synthesis of Tetrazoles. A mixture of benzaldehyde oxime (1.0 mmol), NaN₃ (1.5 mmol), K₂CO₃ (3.0 mmol), and Ni(OH)₂ NPs (4 mg, 4.32 mol %) in water (3 mL) was refluxed for 10 h under air. Then, after cooling to room temperature and separation of the catalyst, the reaction mixture was treated with 5 mL HCl (4.5 M) followed by extracted with ethyl acetate (3 × 10 mL). The organic part was washed with brine, dried over Na₂SO₄ (anhy.), and evaporated to leave the crude product, which was purified by column chromatography over silica gel with hexane/ethyl acetate as the eluent to furnish pure 5-phenyl-1H-tetrazole (**2a**, yield 98%) as a white solid. ¹H NMR (400 MHz, DMSO-*d*₆): δ 8.04–8.03 (m, 2H), 7.45–7.44 (m, 3H).

4.5. Synthesis of 9-(4-Iodophenyl)-9H-carbazole (Compound 5, Scheme 4). Compound 5 was prepared

following our previously reported methodology.⁸⁶ A mixture of carbazole (1 mmol), 1,4-diiodo benzene (1 mmol), NaOH (1.2 mmol) and biogenic CuO NPs in DMF was heated at 120 °C for 15 h. Then, after cooling, the reaction mixture was taken in ice cold water and extracted using ethyl acetate (3 × 10 mL). The organic part was separated, collected and washed with brine, dried over Na₂SO₄ (anhy.), and evaporated to leave the crude product that was purified by column chromatography to furnish compound **5** (yield 85%) as a white solid. ¹H NMR (400 MHz, CDCl₃): δ 8.01 (d, *J* = 7.2 Hz, 2H), 7.77 (d, *J* = 7.2 Hz, 2H), 7.30–7.24 (m, 4H), 7.19–7.15 (m, 4H).

4.6. Synthesis of 9-(4-(5-(Quinolin-2-yl)-1H-tetrazol-1-yl)phenyl)-9H-carbazole (Compound 6, Scheme 4). A mixture of 9-(4-iodophenyl)-9H-carbazole (compound **5**, 1 mmol), **3d** (1 mmol), K₂CO₃ (2 mmol), *N,N'*-dimethylethylenediamine (20 mol %), and CuI (10 mol %) in *p*-xylene was refluxed for 16 h under air. Then, after cooling to room temperature, the solvent was removed under reduced pressure and the reaction mixture was taken for solvent extraction using water and ethyl acetate (3 × 10 mL). The organic part was separated, collected and washed with brine, dried over Na₂SO₄ (anhy.), and evaporated to leave the crude product, which was purified by column chromatography over silica gel with hexane/ethylacetate (95:5) as eluent to furnish compound **6** (yield 89%) as a yellowish white solid. ¹H NMR (400 MHz, CDCl₃): δ 8.36 (dd, *J* = 16.8, 8.4 Hz, 2H), 8.16 (d, *J* = 8.4 Hz, 1H), 8.08 (d, *J* = 8.0 Hz, 2H), 8.03 (d, *J* = 8.8 Hz, 2H), 7.87 (d, *J* = 8.0 Hz, 1H), 7.79–7.75 (m, 1H), 7.61 (t, *J* = 6.0 Hz, 1H), 7.54 (d, *J* = 8.8 Hz, 2H), 7.36–7.35 (m, 4H), 7.24–7.20 (m, 2H); ¹³C NMR (100 MHz, CDCl₃): δ 162.4, 149.4, 146.3, 141.0, 138.1, 137.0, 133.6, 130.5, 129.7, 129.5, 128.3, 127.9, 125.9, 123.3, 121.1, 120.3, 119.9, 118.8, 109.7; IR value: 3418, 3351, 2921, 2851, 1735, 1681, 1593, 1516, 1449, 1384, 1225, 1126, 833, 755 cm⁻¹. Anal. Calcd for C₂₈H₁₈N₆: C, 76.70; H, 4.14; N, 19.17. Found: C, 76.77; H, 4.01; N, 19.12%.

4.7. General Procedure for the Synthesis of Water-Soluble Tetrazoles. A mixture of formaldehyde oxime (1.0 mmol), NaN₃ (1.5 mmol), K₂CO₃ (3.0 mmol), and Ni(OH)₂ NPs (4 mg, 4.32 mol %) in water (1.5 mL) was refluxed for 18 h. After completion of the reaction (monitored by TLC), the water phase was acidified to pH < 1 with concentrated HCl. Then, the solution was extracted with excess ethyl acetate for five times. Thereafter, the combined organic phase was dried under reduced pressure, and the solid mass was washed with the solvent containing ethyl acetate/hexane mixture (10:90) and then recrystallized from ethyl acetate yielding 1H-tetrazole as colourless solid.

4.8. Spectral Sensing of Hydrogen Peroxide. Compound **6** shows a characteristic UV vis absorption spectrum with a prominent λ_{\max} at 292 nm. It was dissolved in spectroscopic grade methanol to obtain a 0.114 μ M solution (A) for fluorescence studies and a 0.057 μ M solution (B) for UV–vis absorption spectral studies. A stock solution of 490 mM H₂O₂ was prepared for sensing applications. Portions of this stock solution (0.01 mL) were added to 2 mL of the solution A for fluorescence spectral studies, and 0.01 mL portions were added to 2 mL of solution B for UV–vis absorption spectral studies. Further for increasing the sensitivity of the fluorescence sensing method, 1000 times diluted H₂O₂ solution (490 μ M) was added and the emissions were recorded at increasing intervals of time.

4.9. TCSPC Lifetime Spectroscopy. The fluorescence lifetime of the above-mentioned solution of compound **6** and

that of H₂O₂-treated solution were measured by the TCSPC method using a nanosecond laser diode (291 nm) as the light source. An IBH DAS-6 decay analysis software was used for deconvoluting the fluorescence decay pattern. The mean fluorescence lifetimes for the decay curves obtained from the two sets were calculated from the respective decay times. The following equation was used to calculate the average lifetime from the relative contribution of the components.

$$\tau_{av} = \frac{a_i \tau_i^2}{a_i \tau_i} \quad (1)$$

where τ_i represents the decay time of the sample, τ_{av} is the average decay time, and a_i indicates the coefficient of the i th component.

4.10. Cyclic Voltammetry. A 0.114 μ M acetonitrile solution of compound **6** was taken for CV studies against tetrabutylammonium perchlorate as the supporting electrolyte.

■ ASSOCIATED CONTENT

📄 Supporting Information

The Supporting Information is available free of charge on the ACS Publications website at DOI: 10.1021/acsomega.8b01081.

Data and scanned copy of the ¹H NMR and ¹³C NMR spectra of all products; ESI-MS of compound **6**; comparison for the detection of H₂O₂ sensing; comparison of the catalytic activity of Ni(OH)₂ NPs; and FT-IR spectrum of reused catalyst (PDF)

■ AUTHOR INFORMATION

Corresponding Authors

*E-mail: a.singha-roy@aston.ac.uk (A.S.R.).

*E-mail: manir65@rediffmail.com (S.M.I.).

*E-mail: kamalchem.roy@gmail.com (K.S.).

ORCID

Anupam Singha Roy: 0000-0003-4052-272X

Kamalika Sen: 0000-0003-1005-5147

Notes

The authors declare no competing financial interest.

■ ACKNOWLEDGMENTS

M.H., M.M.I., and P.S. express sincere thanks to UGC, New Delhi, for providing UGC-SRF, UGC-MANF-SRF, and UGC-JRF. A.S.R. acknowledges DST-SERB, India and Royal Society, UK for his Newton-Bhabha International postdoctoral fellowship. The authors sincerely thank DST-PURSE for funding toward ESI-MS.

■ REFERENCES

- (1) Subramanian, V.; Knight, J. S.; Parekar, S.; Anguish, L.; Coonrod, S. A.; Kaplan, M. J.; Thompson, P. R. Design, synthesis, and biological evaluation of tetrazole analogs of Cl-amidine as protein arginine deiminase inhibitors. *J. Med. Chem.* **2015**, *58*, 1337–1344.
- (2) Asif, M. Biological potentials of substituted tetrazole compounds. *Pharm. Methods* **2014**, *5*, 39–46.
- (3) Mohite, P. B.; Bhaskar, V. H. Potential pharmacological activities of tetrazoles in the new millennium. *Int. J. Pharm. Tech. Res.* **2011**, *3*, 1557–1566.
- (4) Mohammed, J. H. Biological activities importance of tetrazole derivatives. *Eur. Acad. Res.* **2016**, *3*, 12796–12804.

- (5) Klapotke, T. M.; Piercey, D. G. 1,1'-Azobis(tetrazole): a highly energetic nitrogen-rich compound with a N₁₀ chain. *Inorg. Chem.* **2011**, *50*, 2732–2734.

- (6) Feng, W.; Li, L.; Yang, C.; Welle, A.; Trapp, O.; Levkin, P. A. UV-induced tetrazole-thiol reaction for polymer conjugation and surface functionalization. *Angew. Chem., Int. Ed.* **2015**, *54*, 8732–8735.

- (7) Fischer, D.; Klapotke, T. M.; Stierstorfer, J. 1,5-di(nitramino)-tetrazole: high sensitivity and superior explosive performance. *Angew. Chem., Int. Ed.* **2015**, *54*, 10299–10302.

- (8) Damavarapu, R.; Klapotke, T. M.; Stierstorfer, J.; Tarantik, K. R. Barium salts of tetrazole derivatives-synthesis and characterization. *Propellants, Explos., Pyrotech.* **2010**, *35*, 395–406.

- (9) Frija, L. M. T.; Ismael, A.; Cristiano, M. L. S. Photochemical transformations of tetrazole derivatives: applications in organic synthesis. *Molecules* **2010**, *15*, 3757–3774.

- (10) Hu, H.-C.; Kang, X.-M.; Cao, C.-S.; Cheng, P.; Zhao, B. First tetrazole-bridged d-f heterometallic MOFs with a large magnetic entropy change. *Chem. Commun.* **2015**, *51*, 10850–10853.

- (11) Wang, X.-L.; Li, T.-J.; Tian, A.-X.; Li, N.; Yang, Y.; Ning, Y.-L.; Hou, X. Influence of N-donor sites in 5-(x-pyridyl)-1H-tetrazole ligands (x = 2, 4) on assembly of polyoxometalate-based compounds modified by multinuclear metal clusters and infinite chains. *CrystEngComm* **2015**, *17*, 3257–3267.

- (12) Jursic, B. S.; Leblanc, B. W. Preparation of tetrazoles from organic nitriles and sodium azide in micellar media. *J. Heterocycl. Chem.* **1998**, *35*, 405–408.

- (13) Sandmann, G.; Schneider, C.; Boger, P. Z. A new non-radioactive assay of phytoene desaturase to evaluate bleaching herbicides. *Z. Naturforsch. C Biosci.* **1996**, *51*, 534–538.

- (14) Hantzsch, A.; Vagt, A. Ueber das sogenannte diazoganidin. *Justus Liebigs Ann. Chem.* **1901**, *314*, 339–369.

- (15) Amantini, D.; Beleggia, R.; Fringuelli, F.; Pizzo, F.; Vaccaro, L. TBAF-catalyzed synthesis of 5-substituted 1H-tetrazoles under solventless conditions. *J. Org. Chem.* **2004**, *69*, 2896–2898.

- (16) Yildirim, Y.; Pamir, Ö.; Yavuz, S.; Dişli, A. Synthesis and characterization of new the baine derivatives as potential opioid agonists and antagonists: 2-[N-(1H-Tetrazol-5-yl)-6, 14-endoetheno-6, 7, 8, 14-tetrahydro thebaine-7 α -yl]-5-phenyl-1, 3, 4-oxadiazoles. *J. Heterocycl. Chem.* **2013**, *50*, E93–E99.

- (17) Su, W.-K.; Hong, Z.; Shan, W.-G.; Zhang, X.-X. A facile synthesis of 1-substituted-1H-1,2,3,4-tetrazoles catalyzed by ytterbium triflate hydrate. *Eur. J. Org. Chem.* **2006**, 2723–2726.

- (18) Hajra, S.; Sinha, D.; Bhowmick, M. Metal triflate catalyzed reactions of alkenes, NBS, nitriles, and TMSN₃: synthesis of 1,5-disubstituted tetrazoles. *J. Org. Chem.* **2007**, *72*, 1852–1855.

- (19) Akhlaghinia, B.; Rezazadeh, S. A novel approach for the synthesis of 5-substituted-1H-tetrazoles. *J. Braz. Chem. Soc.* **2012**, *23*, 2197–2203.

- (20) Keith, J. M. One-step conversion of pyridine N-oxides to tetrazolo[1,5-a]-pyridines. *J. Org. Chem.* **2006**, *71*, 9540–9543.

- (21) Venkateshwarlu, G.; Premalatha, A.; Rajanna, K. C.; Saiprakash, P. K. Cadmium chloride as an efficient catalyst for neat synthesis of 5-substituted 1H-tetrazoles. *Synth. Commun.* **2009**, *39*, 4479–4485.

- (22) Shie, J.-J.; Fang, J.-M. Microwave-assisted one-pot tandem reactions for direct conversion of primary alcohols and aldehydes to triazines and tetrazoles in aqueous media. *J. Org. Chem.* **2007**, *72*, 3141–3144.

- (23) Lakshmi Kantam, M.; Kumar, K. B. S.; Sridhar, C. Nanocrystalline ZnO as an efficient heterogeneous catalyst for the synthesis of 5-substituted 1H-tetrazoles. *Adv. Synth. Catal.* **2005**, *347*, 1212–1214.

- (24) Bosch, L.; Vilarrasa, J. Cu₂(OTf)₂-catalyzed and microwave-controlled preparation of tetrazoles from nitriles and organic azides under mild, safe conditions. *Angew. Chem., Int. Ed.* **2007**, *46*, 3926–3930.

- (25) Nasrollahzadeh, M.; Bayat, Y.; Habibi, D.; Moshaei, S. FeCl₃-SiO₂ as a reusable heterogeneous catalyst for the synthesis of 5-

substituted 1*H*-tetrazoles via [2+3] cycloaddition of nitriles and sodium azide. *Tetrahedron Lett.* **2009**, *50*, 4435–4438.

(26) Vorona, S.; Artamonova, T.; Zevatskii, Y.; Myznikov, L. An improved protocol for the preparation of 5-substituted tetrazoles from organic thiocyanates and nitriles. *Synthesis* **2014**, *46*, 781–786.

(27) Matthews, D. P.; Green, J. E.; Shuker, A. J. Parallel synthesis of alkyl tetrazole derivatives using solid support chemistry. *J. Comb. Chem.* **2000**, *2*, 19–23.

(28) Schmidt, B.; Meid, D.; Kieser, D. Safe and fast tetrazole formation in ionic liquids. *Tetrahedron* **2007**, *63*, 492–496.

(29) Wittenberger, S. J.; Donner, B. G. Di-alkyltin oxide mediated addition of trimethylsilyl azide to nitriles. A novel preparation of 5-substituted tetrazoles. *J. Org. Chem.* **1993**, *58*, 4139–4141.

(30) Kivrakidou, O.; Bräse, S.; Hülshorst, F.; Griebenow, N. Solid-phase synthesis of 5-biphenyl-2-yl-1*H*-tetrazoles. *Org. Lett.* **2004**, *6*, 1143–1146.

(31) Jin, T.; Kitahara, F.; Kamijo, S.; Yamamoto, Y. Synthesis of 5-substituted 1*H*-tetrazoles by the copper-catalyzed [3+2] cycloaddition of nitriles and trimethylsilyl azide. *Chem.—Asian J.* **2008**, *3*, 1575–1580.

(32) Bonnamour, J.; Bolm, C. Iron salts in the catalyzed synthesis of 5-substituted 1*H*-tetrazoles. *Chem.—Eur. J.* **2009**, *15*, 4543–4545.

(33) Khan, K. M.; Fatima, I.; Saad, S. M.; Taha, M.; Voelter, W. An efficient one-pot protocol for the conversion of benzaldehydes into tetrazole analogs. *Tetrahedron Lett.* **2016**, *57*, 523–524.

(34) Ghodsinia, S. S. E.; Akhlaghinia, B. A rapid metal free synthesis of 5-substituted-1*H*-tetrazoles using cuttlebone as a natural high effective and low cost heterogeneous catalyst. *RSC Adv.* **2015**, *5*, 49849–49860.

(35) Mani, P.; Sharma, C.; Kumar, S.; Awasthi, S. K. Efficient heterogeneous silver nanoparticles catalyzed one-pot synthesis of 5-substituted 1*H*-tetrazoles. *J. Mol. Catal. A: Chem.* **2014**, *392*, 150–156.

(36) Kazemnejadi, M.; Sardarian, A. R. Ecofriendly synthesis of a heterogeneous polyvinyl alcohol immobilized copper(II) Schiff base complex as an efficient, reusable catalyst for the one-pot three-component green preparation of 5-substituted 1*H*-tetrazoles under mild conditions. *RSC Adv.* **2016**, *6*, 91999–92006.

(37) Esirden, İ.; Erken, E.; Kaya, M.; Sen, F. Monodisperse Pt NPs@rGO as highly efficient and reusable heterogeneous catalysts for the synthesis of 5-substituted 1*H*-tetrazole derivatives. *Catal. Sci. Technol.* **2015**, *5*, 4452–4457.

(38) Abdollahi-Alibeik, M.; Moaddeli, A. Cu-MCM-41 nanoparticles: an efficient catalyst for the synthesis of 5-substituted 1*H*-tetrazoles via [3+2] cycloaddition reaction of nitriles and sodium azide. *J. Chem. Sci.* **2016**, *128*, 93–99.

(39) Shahbazali, E.; Hessel, V.; Noël, T.; Wang, Q. Metallic nanoparticles made in flow and their catalytic applications in organic synthesis. *Phys. Sci. Rev.* **2016**, *1*, 16.

(40) Mitrofanov, A. Y.; Murashkina, A. V.; Martín-García, I.; Alonso, F.; Beletskaya, I. P. Formation of C–C, C–S and C–N bonds catalysed by supported copper nanoparticles. *Catal. Sci. Technol.* **2017**, *7*, 4401–4412.

(41) Narayanan, R. Synthesis of green nanocatalysts and industrially important green reactions. *Green Chem. Lett. Rev.* **2012**, *5*, 707–725.

(42) Zhang, X.; Shi, W.; Zhu, J.; Zhao, W.; Ma, J.; Mhaisalkar, S.; Maria, T. L.; Yang, Y.; Zhang, H.; Hng, H. H.; Yan, Q. Synthesis of porous NiO nanocrystals with controllable surface area and their application as supercapacitor electrodes. *Nano Res.* **2010**, *3*, 643–652.

(43) Xia, J.; He, G.; Zhang, L.; Sun, X.; Wang, X. Hydrogenation of nitro phenols catalyzed by carbon black-supported nickel nanoparticles under mild conditions. *Appl. Catal., B* **2016**, *180*, 408–415.

(44) Abrishami, F.; Ebrahimikia, M.; Rafiee, F. Synthesis of 5-substituted 1*H*-tetrazoles using a recyclable heterogeneous nanonickel ferrite catalyst. *Appl. Organomet. Chem.* **2015**, *29*, 730–735.

(45) Ghorbani-Choghamarani, A.; Taherinia, Z. High catalytic activity of peptide nanofibres decorated with Ni and Cu nanoparticles for the synthesis of 5-substituted 1*H*-tetrazoles and N-arylation of amines. *Aust. J. Chem.* **2017**, *70*, 1127–1137.

(46) Ghorbani-Choghamarani, A.; Moradi, P.; Tahmasbi, B. Ni–S-methyl isothiourae complexes supported on boehmite nanoparticles and their application in the synthesis of 5-substituted tetrazoles. *RSC Adv.* **2016**, *6*, 56638–56646.

(47) Tamoradi, T.; Mehraban-Esfandiari, B.; Ghadermazi, M.; Ghorbani-Choghamarani, A. Immobilization of a nickel complex onto functionalized Fe₃O₄ nanoparticles: a green and recyclable catalyst for synthesis of 5-substituted 1*H*-tetrazoles and oxidation reaction. *Res. Chem. Intermed.* **2018**, *44*, 1363–1380.

(48) Safaei-Ghomi, J.; Paymard-Samani, S. Facile and rapid synthesis of 5-substituted 1*H*-tetrazoles via a multicomponent domino reaction using nickel(II) oxide nanoparticles as catalyst. *Chem. Heterocycl. Compd.* **2015**, *50*, 1567–1574.

(49) Islam, M. M.; Halder, M.; Roy, A. S.; Islam, S. M. Heterogeneous route for the one-pot synthesis of N-arylamides from aldoximes and aryl halides using the CuO/carbon material. *ACS Omega* **2017**, *2*, 8600–8609.

(50) De, P.; Nonappa; Pandurangan, K.; Maitra, U.; Wailes, S. Cu-mediated cross-coupling of aryl halides with oximes: a direct access to O-aryloximes. *Org. Lett.* **2007**, *9*, 2767–2770.

(51) Lin, M.-H.; Lin, L.-Z.; Chuang, T.-H.; Liu, H.-J. One-pot sequential deoximation and allylation reactions of aldoximes in aqueous solution. *Tetrahedron* **2012**, *68*, 2630–2635.

(52) Patil, U. B.; Kumthekar, K. R.; Nagarkar, J. M. A novel method for the synthesis of 5-substituted 1*H*-tetrazole from oxime and sodium azide. *Tetrahedron Lett.* **2012**, *53*, 3706–3709.

(53) Guggilapu, S.; Prajapati, S.; Nagarsenkar, A.; Gupta, K.; Babu, B. Indium(III) chloride catalyzed synthesis of 5-substituted 1*H*-tetrazoles from oximes and sodium azide. *Synlett* **2016**, *27*, 1241–1244.

(54) Ishihara, K.; Kawashima, M.; Shioiri, T.; Matsugi, M. Synthesis of 5-substituted 1*H*-tetrazoles from aldoximes using diphenyl phosphorazidate. *Synlett* **2016**, *27*, 2225–2228.

(55) Matos, R. C.; Coelho, E. O.; de Souza, C. F.; Guedes, F. A.; Matos, M. A. C. Peroxidase immobilized on amberlite IRA-743 resin for on-line spectrophotometric detection of hydrogen peroxide in rainwater. *Talanta* **2006**, *69*, 1208–1214.

(56) Yue, H.; Bu, X.; Huang, M.-H.; Young, J.; Raglione, T. Quantitative determination of trace levels of hydrogen peroxide in crospovidone and a pharmaceutical product using high performance liquid chromatography with coulometric detection. *Int. J. Pharm.* **2009**, *375*, 33–40.

(57) Chen, S.; Yuan, R.; Chai, Y.; Hu, F. Electrochemical sensing of hydrogen peroxide using metal nanoparticles: a review. *Microchim. Acta* **2013**, *180*, 15–32.

(58) Lou, X.; Zhu, C.; Pan, H.; Ma, J.; Zhu, S.; Zhang, D.; Jiang, X. Cost-effective three-dimensional graphene/Ag aerogel composite for high-performance sensing. *Electrochim. Acta* **2016**, *205*, 70–76.

(59) Chen, S.-X.; Schopfer, P. Hydroxyl-radical production in physiological reactions. a novel function of peroxidase. *Eur. J. Biochem.* **1999**, *260*, 726–735.

(60) Quintanilla, A.; Casas, J. A.; Rodriguez, J. J. Hydrogen peroxide-promoted-CWAO of phenol with activated carbon. *Appl. Catal., B* **2010**, *93*, 339–345.

(61) Chen, W.; Cai, S.; Ren, Q.-Q.; Wen, W.; Zhao, Y.-D. Recent advances in electrochemical sensing for hydrogen peroxide: a review. *Analyst* **2012**, *137*, 49–58.

(62) Wang, L.; Deng, M.; Ding, G.; Chen, S.; Xu, F. Manganese dioxide based ternary nanocomposite for catalytic reduction and nonenzymatic sensing of hydrogen peroxide. *Electrochim. Acta* **2013**, *114*, 416–423.

(63) Rhee, S. G. Cell signaling, H₂O₂ a necessary evil for cell signaling. *Science* **2006**, *312*, 1882–1883.

(64) Halliwell, B.; Clement, M. V.; Long, L. H. Hydrogen peroxide in the human body. *FEBS Lett.* **2000**, *486*, 10–13.

(65) Lacy, F.; O'Connor, D. T.; Schmid-Schonbein, G. W. Plasma hydrogen peroxide production in hypertensive and normotensive subjects at genetic risk of hypertension. *J. Hypertens.* **1998**, *16*, 291–303.

(66) Deskur, E.; Przywarska, I.; Dylewicz, P.; Szczeńsiak, Ł.; Rychlewski, T.; Wilk, M.; Wysocki, H. Exercise-induced increase in hydrogen peroxide plasma levels is diminished by endurance training after myocardial infarction. *Int. J. Cardiol.* **1998**, *67*, 219–224.

(67) Reddy, J. K.; Rao, M. S. Oxidative DNA damage caused by persistent peroxisome proliferation: its role in hepatocarcinogenesis. *Mutat. Res.* **1989**, *214*, 63–68.

(68) Halliwell, B.; Gutteridge, J. M. C. *Free Radicals in Biology and Medicine*, 3rd ed.; Clarendon Press: Oxford, 1999.

(69) Harman, D. Aging: a theory based on free radical and radiation chemistry. *J. Gerontol.* **1956**, *11*, 298–300.

(70) Behl, C.; Davis, J. B.; Lesley, R.; Schubert, D. Hydrogen peroxide mediates amyloid beta protein toxicity. *Cell* **1994**, *77*, 817–827.

(71) Miyata, M.; Smith, J. D. Apolipoprotein E allele-specific antioxidant activity and effects on cytotoxicity by oxidative insults and beta-amyloid peptides. *Nat. Genet.* **1996**, *14*, 55–61.

(72) Lo, K. W. K.; Liu, H. W.; Lee, C. C. U.S. Patent Appl. Publ. US 20170114275 A1, April 27, 2017.

(73) Claussen, J. C.; Franklin, A. D.; Fisher, T. S.; Porterfield, D. M. U.S. Pat. Appl. Publ. US 20100285514 A1, Nov 11, 2010.

(74) Voraberger, H. Optical Techniques for Determination and Sensing of Hydrogen Peroxide in Industrial and Environmental Samples. In *Optical Sensors: Industrial, Environmental and Diagnostic Applications*; Narayanaswamy, R., Wolfbeis, O. S., Eds.; Springer: Berlin, London, 2004; pp 391–408.

(75) Liu, F.; Bing, T.; Shangguan, D.; Zhao, M.; Shao, N. Ratio metric fluorescent biosensing of hydrogen peroxide and hydroxyl radical in living cells with lysozyme-silver nanoclusters: lysozyme as stabilizing ligand and fluorescence signal unit. *Anal. Chem.* **2016**, *88*, 10631–10638.

(76) Kong, L.; Ren, Z.; Zheng, N.; Du, S.; Wu, J.; Tang, J.; Fu, H. Interconnected 1D Co₃O₄ nanowires on reduced graphene oxide for enzymeless H₂O₂ detection. *Nano Res.* **2015**, *8*, 469–480.

(77) Wang, G.; Xu, J.-J.; Chen, H.-Y.; Lu, Z.-H. Amperometric hydrogen peroxide biosensor with sol-gel/chitosan network-like film as immobilization matrix. *Biosens. Bioelectron.* **2003**, *18*, 335–343.

(78) Palanisamy, S.; Chen, S.-M.; Sarawathi, R. A novel non-enzymatic hydrogen peroxide sensor based on reduced graphene oxide/ZnO composite modified electrode. *Sens. Actuators, B* **2012**, *166–167*, 372–377.

(79) Urano, Y.; Kamiya, M.; Kanda, K.; Ueno, T.; Hirose, K.; Nagano, T. Evolution of fluorescein as a platform for finely tunable fluorescence probes. *J. Am. Chem. Soc.* **2005**, *127*, 4888–4894.

(80) Abo, M.; Urano, Y.; Hanaoka, K.; Terai, T.; Komatsu, T.; Nagano, T. Development of a highly sensitive fluorescence probe for hydrogen peroxide. *J. Am. Chem. Soc.* **2011**, *133*, 10629–10637.

(81) Meulenkamp, E. A. Size dependence of the dissolution of ZnO nanoparticles. *J. Phys. Chem. B* **1998**, *102*, 7764–7769.

(82) Kida, T.; Oka, T.; Nagano, M. Synthesis and application of stable copper oxide nanoparticle suspensions for nanoparticulate film fabrication. *J. Am. Ceram. Soc.* **2007**, *90*, 107–110.

(83) Qi, Y.; Qi, H.; Li, J.; Lu, C. Synthesis, microstructures and UV-vis absorption properties of β -Ni(OH)₂ nanoplates and NiO nanostructures. *J. Cryst. Growth* **2008**, *310*, 4221–4225.

(84) Bortolini, O.; De Nino, A.; Fogagnolo, M.; Fantin, G.; Mariuolo, L.; Tocci, A. Oxidative cleavage of nitroalkenes with hydrogen peroxide in environmentally acceptable solvents. *Chem. Lett.* **2007**, *36*, 472–473.

(85) Kadyrov, R.; Hackenberger, D. Oxidative cleavage of long chain olefins to carboxylic acids with hydrogen peroxide. *Top. Catal.* **2014**, *57*, 1366–1371.

(86) Halder, M.; Islam, M. M.; Ansari, Z.; Ahammed, S.; Sen, K.; Islam, S. M. Biogenic nano-CuO-catalyzed facile C–N cross-coupling reactions: scope and mechanism. *ACS Sustainable Chem. Eng.* **2017**, *5*, 648–657.